ELSEVIER

Journal of Power Sources 87 (2000) 106–111

JOURNAL OF POWER SOURCES

www.elsevier.com/locate/jpowsour

# Use of amorphous tin-oxide films obtained by spray pyrolysis as electrodes in lithium batteries

R. Ayouchi [a], F. Martin [b], J.R. Ramos Barrado [a], M. Martos [c], J. Morales [c,*], L. Sánchez [c]

[a] *Departamento de Física Aplicada, Facultad de Ciencias, Campus de Teatinos, Universidad de Málaga, Málaga, Spain*
[b] *Departamento de Ingeniería Química, Facultad de Ciencias, Campus de Teatinos, Universidad de Málaga, Málaga, Spain*
[c] *Laboratorio de Química Inorgánica, Facultad de Ciencias, Universidad de Córdoba, Avenida San Alberto Magno s / n, 14004 Córdoba, Spain*

Received 14 July 1999; accepted 16 September 1999

**Abstract**

Amorphous tin-oxide films were prepared by spray pyrolysis of $SnCl_2 \cdot 2H_2O$ mixed with $CH_3$–COOH and deposited onto a stainless steel substrate at mild temperatures (350°C). The films grown were characterized by X-ray photoelectron spectroscopy (XPS) and scanning electron microscopy with energy-dispersive X-ray analysis (SEM-EDX). Also, they were tested as electrodes in lithium rechargeable batteries. The XPS results suggest that the substrate is thoroughly coated and that the films are composed mainly of SnO and $SnO_2$. These films exhibit good charge–discharge properties over more than 100 cycles. Heating at 600°C causes significant changes in their surface composition, in the virtual disappearance of the tin component and in the presence of oxygen-bound Fe. Under these conditions, the reversible capacity dramatically fades and the cell behaves similarly to that made from uncoated substrate. 

*Keywords:* Lithium; Lithium-ion batteries; Tin oxide; Thin film

## 1. Introduction

Ever since the announcement by Fuji Film researchers a few years ago that Sn-based composite oxides [1] can yield a reversible Li-ion storage capacity above 600 mA h/g, much research has been conducted with the aim of elucidating relevant structural aspects of the underlying mechanism for the electrochemical reaction [2–8], as well as other factors related to the influence of heat treatment in the preparation of the $SnO_2$ electrode [9] and the role played by different doping elements [10,11]. Thin film methods for the preparation of tin oxide-based electrodes, either amorphous or crystalline, have been also used [12,13]. Although the electrochemical performance of the cells tested so far is described as excellent [12] and indeed promising, the methods used for this purpose, viz. chemical vapor deposition (CVD) [12] and electron-beam evaporation [13], are expensive inasmuch as they require rather sophisticated equipment. In this context, the spray pyrolysis method is a simple, inexpensive alternative with the added advantage that it allows large films to be prepared [14].

The purpose of this research was to explore the usefulness of the spray pyrolysis method for obtaining tin-oxide films with a view to examining their potential as negative electrodes for lithium-ion batteries. In this paper, we report the preliminary results obtained regarding the performance of the cells, and the characterization of the films by using different techniques, namely: X-ray diffraction (XRD), X-ray photoelectron spectroscopy (XPS) and scanning electron microscopy (SEM) with energy-dispersive X-ray analysis (EDX).

## 2. Experimental

In our technique, compressed air is used to atomize a solution containing the precursor compounds through a spray nozzle over the heated substrate (Fig. 1). Air is directly compressed from the atmosphere, using filters to remove water and oil waste in order to obtain films of large surface areas at reduced costs. The precursor was pyrolyzed on the heated substrate. The substrate holder

* Corresponding author. Tel.: +34-957-21-86-21; fax: +34-21-86-06-14004; e-mail: iq1mopaj@uco.es

0378-7753/00/$ - see front matter 
PII: S0378-7753(99)00435-8

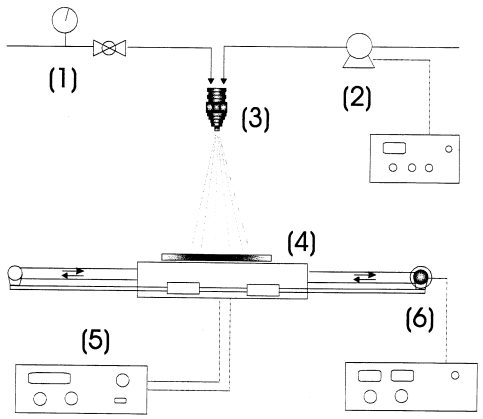


Fig. 1. Spray pyrolysis system used to prepare the films. (1) Compressed air supply. (2) Syringe pump and controller. (3) Spray nozzle. (4) Substrate holder. (5) Temperature controller. (6) Step motor and controller.

was equipped with thermocouples and heating elements. The heating elements were managed by a temperature controller. The substrate was moved forward and backward at a fixed frequency by an electronically controlled step motor. We used aqueous solutions of $SnCl_2$ as precursors and 0.035 M acetic acid to stabilize them. The solutions were pumped into the air stream in the spray nozzle at a variable rate for a preset time by means of a syringe pump. A stream of 140 l/min of air, measured under atmospheric conditions, was used to atomize the solution. Meanwhile, the substrate was kept at 350°C. The substrate size uniformly coated in this way was 2 cm long by 1 cm wide. The deposition time and the rate of the precursor solution were elected in such a way as to obtain the same amount of tin oxide on the substrate. The deposition conditions for the two films are shown in Table 1.

X-ray photoelectron spectra were obtained on a Physical Electronics PHI 5700 spectrometer using unmonochromatized Mg K$\alpha$ radiation (1253.6 eV) as excitation source. The spectrometer was calibrated by assuming the binding energy (BE) of the Au $4f_{7/2}$ line at 84.0 eV with respect to the Fermi level. The PHI ACCESS.ESCA-V6.0F software package was used for data acquisition and analysis. After Shirley-type background subtraction, spectra were fitted using a Gaussian–Lorentzian peak shape for all peaks.

SEM images were obtained on Jeol JMS 6400 microscope equipped with an EDX microanalysis system.

Table 1
Spray pyrolysis deposition conditions

| Sample | Spray sol. conc. (mM) | Carrier flow rate (ml/h) | Deposition time (min) | Total vol. sol. sprayed ($cm^3$) |
|---|---|---|---|---|
| A | 5 | 50 | 30 | 25 |
| B | 5 | 100 | 15 | 25 |

Electrochemical experiments were carried out in two-electrode cells, using lithium as anode. The electrolyte used was 1 M anhydrous $LiPF_6$ in a 1:1 mixture of ethylene carbonate (EC) and dimethyl carbonate (DMC). The thin film of the active material was cut in squares of $4 \times 4$ mm and lithium foil was cut as circles of 7-mm diameter. Unless otherwise noted, cells were cycled at a 0.25 $mA/cm^2$ current density, controlled via a MacPile II potentiostat–galvanostat.

## 3. Results and discussion

Under the above-mentioned conditions, and the substrate at 350°C, the films obtained were amorphous in all cases — the XRD patterns only exhibited peaks belonging to the substrate. More valuable information was obtained from the XPS results. It is difficult to precisely measure the BE for these films owing to charging effects. Also, the method based on C 1s impurity peak, belonging to adventitious hydrocarbon (C 1s 284.8 eV) for calibration could not be directly applied as the C 1s spectrum for the two samples was asymmetric and broadened. In fact, C 1s spectra were resolved into three components at $284.9 \pm 0.1$, $286.6 \pm 0.2$ and $289.1 \pm 0.1$ eV. We assumed the lower BE peak to correspond to adventitious hydrocarbon in addition to the methyl group of undecomposed impurities of acetic acid, as shown below, and used it as internal standard for the peak positions shown in Table 2. The weaker and higher BE peaks at 286.6 and 289.1 eV are similar to those reported for C–O in organic alcohols and C=O in ketones, respectively [15].

All O 1s spectra exhibited complex profiles that were fitted into two peaks at about 531 and 532 eV, the lower BE peak being stronger than the higher one. The profile complexity is indicative of the presence of different oxygen types at the film surface, which hinder the accurate determination of the amount of oxygen directly bound to Sn atoms.

The Sn 3d photoemission signals were symmetric for the two samples. The fact that BE was constant (see Table 2) means that no change in its oxidation state could be identified in each case. A comparison of its BE with that

Table 2
Binding energies for the main core level spectra (eV). The values in bracket are percent area

| | Sample A | Sample B |
|---|---|---|
| C 1s | 284.8 (81.5) | 284.8 (85.6) |
| | 286.5 (9.7) | 286.4 (10.3) |
| | 289.0 (8.8) | 289.0 (4.0) |
| O 1s | 531.0 (60.0) | 531.0 (68.8) |
| | 532.3 (39.9) | 532.4 (31.1) |
| Sn $3d_{5/2}$ | 487.1 | 487.0 |
| Sn $3d_{3/2}$ | 495.5 | 495.4 |

Table 3
Surface atomic concentrations of films deposited at 350°C (in %)

| | Sample A | Sample B |
|---|---|---|
| C | 31.1 | 44.7 |
| O | 44.9 | 36.3 |
| Sn | 22.9 | 18.1 |
| Cl | 1.1 | 0.9 |

reported for tin oxides by Willeemen et al. [16] revealed the best agreement to correspond to SnO (BE Sn $3d_{5/2}$ 486.9 eV). The reported BE for $SnO_2$ is somewhat lower (486.7 eV). However, values as low as 486.0 eV have also been reported for SnO [17].

The atomic concentration of the elements, determined by considering the corresponding area sensitivity factors [14] for the different measured spectral regions, are shown in Table 3. In addition to C, O, and Sn, traces of Cl were detected; its concentration, however, barely reached 1%, so, it can only have a modest role in Li uptaking. An interesting result of this analysis is the absence of peaks belonging to the substrate components (mainly Fe and Cr). This means that the substrates are thoroughly coated with the deposited material.

The composition data of Table 3 warrant some comments. First, a significant carbon content is observed that is higher for sample B. This suggests that spray pyrolytic deposition at 350°C produces films that are incompletely pyrolyzed. Second, the Sn concentration in sample A is somewhat higher than that calculated for sample B, even though the amount of precursor used was the same. The O/Sn atomic ratio was close to 2 for both samples. However, one should take this value cautiously owing to the presence of unpyrolyzed material in the films and to the asymmetry of the O 1s spectra. On the assumption that stronger component of the oxygen reflects the amount of oxygen directly bound to Sn more accurately, the calculated O/Sn ratio ranged from 1.21 for sample A to 1.38 for sample B. Accordingly, tin atoms on the film surface should be in a mixed valence state [Sn(II) and Sn (IV)]. Unfortunately, these mixed-valence species are not revealed as a fine structure in the Sn 3d photoelectronic peak. In any case, the identification of mixed-valence species by XPS is a subject under debate owing to the many factors that affect the chemical shifts [18].

The SEM images, Fig. 2a, show that the precursor deposits on the substrate as separate droplets with of highly homogenous size (approximately 20 μm). That results in apparently incomplete coating of the steel surface. In order to reconcile the SEM images with XPS results, where no peaks for the substrate constituents were observed, the droplets must be interconnected by a layer of deposited material of thickness at least greater than the attenuation depth of photoelectrons (within 20–50 Å). The images obtained at a higher magnification, Fig. 2b, reveal that the grains formed within the droplets are loosely compacted, and nonuniform in shape and size. In fact, the dry droplets usually behave as illustrated in Fig. 2b, which resembles a crater-like picture; the films thus obtained have a very rough appearance and an extended surface area. On further heating in air at 600°C for 1 h, the films preserved their droplet morphology (Fig. 2c) and amorphous nature. However, the grains tended to increase in size. The images recorded at higher magnifications, (Fig. 2d), exhibit significant changes in surface morphology: the grains are formed by agglomerates of particles in rod-like shaped and lengths smaller than 1 μm.

Attempts to measure the film thickness by SEM with accuracy failed because they were too thin and irregular to obtain a precise value. Moreover, the XPS deep profile

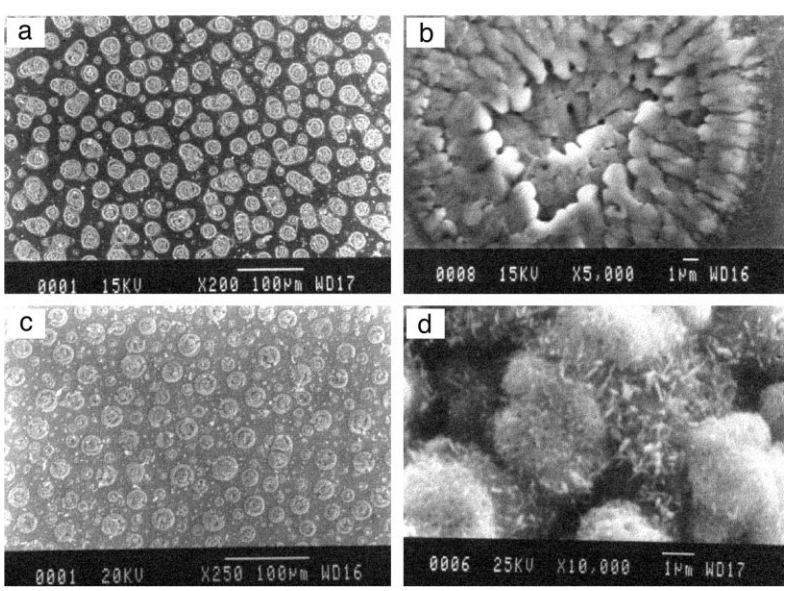


Fig. 2. SEM images of tin oxide films: (a) and (b) films deposited onto the substrate at 350°C; (c) and (d) films heated at 600°C for 1 h.

measurement has the problem of a poor lateral resolution. Owing to the lack of surface homogeneity, the XPS deep profile detects tin and iron without a clear interface. Nevertheles, the film thickness estimated was of the order of 0.5–1.0 μm.

Fig. 3a shows the first discharge curve for the Li/sample B cell, recorded at a current density of 0.25 mA/cm$^2$. Owing to non-uniformity in the coating and to the difficulty of identifying the phases present, the method commonly used to calculate the active material weight based on an assumed density was unsuitable. For this reason, the cell capacity is expressed on a time scale and the cell performance on cycling is referred to the charge curve at maximum capacity (see below). The profile recorded over the voltage range 2.8–0.0 V contains two pseudoplateaux typical of the tin oxide–lithium system, the first one being associated to the initial formation of Sn and the second, below 0.5 V, to the formation of an $Li_xSn$ alloy [3]. The figure also shows other recharge–discharge curves obtained between the limits 1.0 and 0.0 V, the voltage where the capacity loss was the lowest. Over this voltage range, the profiles of both curves are similar, so the reaction between Li and Sn must be a reversible process. This is more clearly seen by analyzing the differential specific capacity plots in Fig. 3b, where the reversibility of the oxidation–reduction process is apparent from the anodic and cathodic waves. Moreover, the broad peaks resulting from the reduction and oxidation reactions contrast with the two sharp peaks overlapped with to the broad peak reported for electron beam-deposited tin-oxide thin films [13], which have ascribed to a phase transition reaction.

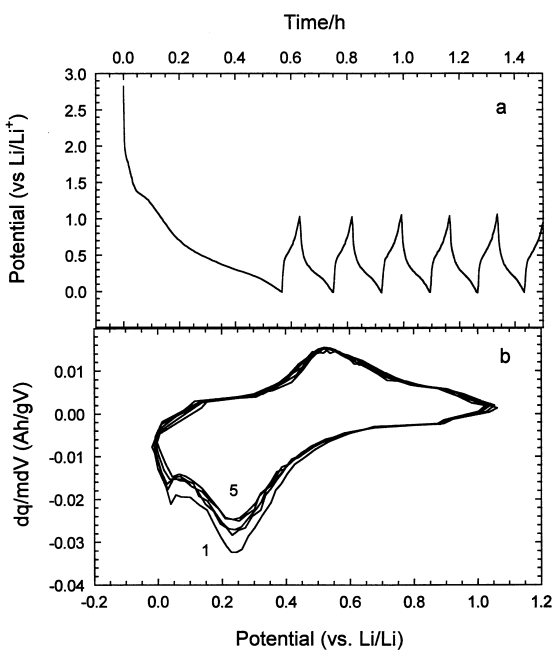


Fig. 3. (a) First discharge curve and subsequent charge–discharge curves for the Li/sample B cell. (b) Differential capacity plots for the first five cycles.

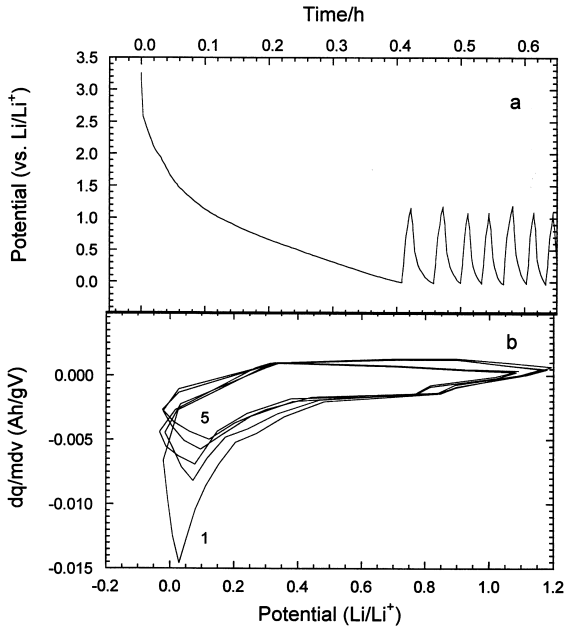


Fig. 4. (a) First discharge curve and subsequent charge–discharge curves for the cell made from uncoated substrate. (b) Differential capacity plots for the first five cycles.

The profiles of Fig. 3b are in better agreement with that for a mixture of $SnO_2$ and SnO when cycled between 0.0 and 0.8 V [2], which is quite consistent with the O/Sn ratio obtained from the XPS data. In order to confirm that virtually the whole cell capacity is generated by the active material, these measurements were extended to a cell the cathode of which was made from the pure substrate. The discharge curve, Fig. 4a, shows that the stainless steel reacts with lithium; however, its shape differs from that of the film in two main respects (Fig. 3a), namely: (i) the discharge depth is smaller and (ii) the two pseudoplateaux associated to tin reduction are virtually absent. In fact, the potential decreases almost linearly with increasing time below 1 V. Moreover, the reaction with lithium is irreversible, as the specific capacity of this cell markedly drops in the first charge process. The differential capacity plots, Fig. 4b, confirm the irreversible behavior of the electrode. The reduction peak, which appears below 0.2 V,

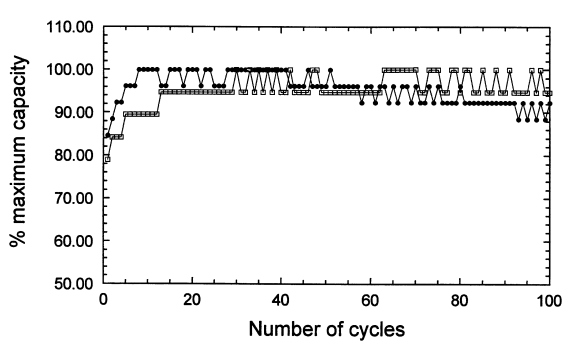


Fig. 5. Cycling performance of tin oxide films: (●) sample A; (□) sample B.

Table 4
Surface atomic concentrations of the films heated at 600°C (in %)

| | Sample A | Sample B |
|---|---|---|
| C | 5.3 | 5.8 |
| O | 56.9 | 58.8 |
| Sn | 3.0 | 0.5 |
| Fe | 34.2 | 34.5 |
| Cl | 0.4 | 0.3 |

is virtually absent in the oxidation curve, thus indicating that the $Li_x$(Fe–Cr) alloy formed on discharge is irreversible. Thus, the role of the substrate in the reversible capacity of the cell made from the film is insubstantial. However, the initial lithium insertion into the stainless steel substrate plays a role in the large first discharge curve observed for the Li/sample B cell (Fig. 3a) and accounts for the shortening in the first charge curve, ascribed to the reversible extraction of lithium from the $Li_xSn$ system. This assumption is not in contradiction with the above comments, because only one face of the substrate was coated by the active tin-oxide material. Thus, the Li insertion into the stainless steel should occur at the uncoated face, which is in direct contact with both the electrolyte and the current collector.

Fig. 5 illustrates the cycling performance of the two cells. The best results were obtained for sample B, the capacity of which remained fairly constant upon extended cycling. The Li retention in the active material observed in the first few cycles and its release on further cycling has been also found in other systems (e.g., submicrocrystalline Sn and SnSb powders [19]). It has been associated to an increase in the electrode–electrolyte interface area which facilitates Li diffusion. The cycling behavior of sample A is worse, particularly beyond the 50th cycle, where the capacity begins to drop. In any case, this cell retains nearly 90% of its maximum delivered capacity.

The capacity of the films annealed at 600°C dramatically faded; also their electrochemical behavior resembled that of the substrate, irrespective of the synthesis conditions used. This is a somewhat surprising result relative to the films prepared by Nam et al. [13] using electron beam evaporation, where the heat treatment had a beneficial effect. These data cannot be explained in morphological or grain size terms. The film surface basically maintains its droplet appearance and particle size decreases on heating, which boosts cell performance. The origin of this behavior contradictory apparently is revealed by the XPS results. The atomic concentrations obtained are shown in Table 4. A comparison with the values in Table 3 reveals three main differences, namely: (i) a decrease in carbon content promoted by the thorough pyrolysis of the organic component; (ii) an increase in oxygen content; and, specially, (iii) a strong appearance of Fe and a negligible concentration of Sn at surface level. This means that the latter element migrates to the bulk substrate, thereby escaping from the X-ray beam. Simultaneously, Fe is extruded to the surface. Under these conditions, the cell behavior is similar to that exhibited by the pure substrate. This was also confirmed by the EDX microanalysis, so Sn atoms can diffuse into the substrate over long distances from the surface (more than 1 μm in depth, which is the attenuation depth for this analytical technique).

## 4. Conclusions

Amorphous tin-oxide films were prepared by spray pyrolysis from aqueous solutions of $SnCl_2 \cdot 2H_2O$ acidified with acetic acid and deposited on stainless steel substrates at 350°C. SEM images revealed that the precursor is deposited as separate droplets of regular size; on contact with the heated substrate, however, the surface become rather rough and the film highly porous. Although the films appear to vary in thickness, no peaks for Fe or Cr are detected by XPS, which indicates that the substrate surface is completely covered by the precursor. XPS data are also consistent with high carbon contents that probably result from the presence of some unpyrolyzed precursor. The oxygen/tin ratio is approximately 1.3, so the films consist of a $SnO/SnO_2$ mixed phase. These films were tested as electrodes in lithium cells, where they exhibited good cycling properies upon extended cycles. Heating the films at 600°C suppressed their reversible capacity through migration of tin to the bulk substrate.

## Acknowledgements

This work was supported by Spain's Ministerio de Educación y Cultura (CICyT Project PB95-0561) and by Junta de Andalucía (Group FQM-175).

## References

[1] Y. Idota, T. Kubota, A. Matsufuji, Y. Maekawa, T. Miyasaka, Science 276 (1997) 1395.
[2] I.A. Courtney, J.R. Dahn, J. Electrochem. Soc. 144 (1997) 2045.
[3] I.A. Courtney, J.R. Dahn, J. Electrochem. Soc. 144 (1997) 2943.
[4] S. Machill, T. Shodai, Y. Sakurai, J. Yamaka, J. Solid State Electrochem. 3 (1999) 97.
[5] T. Brousse, D. Defives, L. Pasquereau, S.M. Lee, U. Herterich, D.M. Schleich, Ionics 3 (1997) 332.
[6] I.A. Courtney, W.R. Mckinnon, J.R. Dahn, J. Electrochem. Soc. 146 (1999) 59.
[7] Y. Wang, J. Sakamoto, C.K. Huang, S. Surampidi, S.G. Greenbaum, Solid State Ionics 110 (1998) 167.
[8] H. Li, H. Huang, L. Chen, Electrochem. Solid-State Lett. 1 (1998) 241.
[9] W. Liu, X. Huang, Z. Wang, H. Li, L. Chen, J. Electrochem. Soc. 145 (1998) 59.
[10] J. Morales, L. Sánchez, J. Electrochem. Soc. 146 (1999) 1640.
[11] J. Morales, L. Sánchez, Solid State Ionics 126 (1999) 219.

[12] T. Brousse, R. Retoux, U. Herterich, D.M. Schleich, J. Electrochem. Soc. 145 (1998) 1.
[13] S.C. Nam, Y.H. Kim, W.Y. Cho, B.W. Cho, H.S. Chun, K.S. Yun, Electrochem. Solid-State Lett. 2 (1999) 9.
[14] S.Y. Park, Y.C. Son, W.S. Willis, S.L. Suib, K.S. Creasy, Chem. Mater. 10 (1998) 2389.
[15] J.F. Moulder, W.F. Stickle, P.E. Sobol, K.D. Bomben, in: J. Chastain (Ed.), Handbook of X-ray Photoelectron Spectroscopy, Perkin-Elmer Physical Electronic Division, Minnesota, 1992.
[16] H. Willeemen, T.S. Vandevondel, G.T. Van deer Kelen, Inorg. Chim. Acta 34 (1977) 175.
[17] R.O. Ansell, T. Dickinson, A.F. Povey, P.M.A. Sherwood, J. Electron. Spectrosc. Relat. Phenom. 11 (1977) 311.
[18] B.D. Ratner, D.G. Castner, Surface Analysis: The Principal Techniques, in: J.C. Vickerman (Ed.), John, New York, 1997, p. 50.
[19] J. Yang, M. Wachtter, M. Winter, J.O. Besenhard, Electrochem. Solid-State Lett. 2 (1999) 161.